

Source-structure trade-offs in ambient noise correlations

Andreas Fichtner

Department of Earth Sciences, ETH Zurich, Zurich, Switzerland. E-mail: andreas.fichtner@erdw.ethz.ch

Accepted 2015 April 27. Received 2015 April 27; in original form 2015 March 4

SUMMARY

We analyse the physics and geometry of trade-offs between Earth structure and noise sources in interstation noise correlations. Our approach is based on the computation of off-diagonal Hessian elements that describe the extent to which variations in noise sources can compensate for variations in Earth structure without changing the misfit beyond the measurement uncertainty. Despite the fact that all ambient noise inverse problems are special in terms of their receiver configuration and data, some general statements concerning source-structure trade-offs can be made: (i) While source-structure trade-offs may be reduced to some extent by clever measurement design, there are inherent trade-offs that can generally not be avoided. These inherent trade-offs may lead to a mispositioning of structural heterogeneities when the noise source distribution is unknown. (ii) When attenuation is weak, source-structure trade-offs in ambient noise correlations are a global phenomenon, meaning that there is no noise source perturbation that does not trade-off with some Earth structure, and vice versa. (iii) The most significant source-structure trade-offs occur within two elliptically shaped regions connecting a potential noise source perturbation to each one of the receivers. (iv) Far from these elliptical regions, only small-scale structure can trade off against changes in the noise source. (v) While source-structure trade-offs mostly decay with increasing attenuation, they are nearly unaffected by attenuation when the noise source perturbation is located near the receiver-receiver line. This work is intended to contribute to the development of joint source-structure inversions of ambient noise correlations, and in particular to an understanding of the extent to which source-structure trade-offs may be reduced. It furthermore establishes the foundation of future resolution analyses that properly quantify trade-offs between noise sources and Earth structure.

Key words: Inverse theory; Tomography; Interferometry; Computational seismology.

1 INTRODUCTION

Over the last decade, seismic tomography based on interstation correlations of ambient noise has developed into a standard tool for exploring and monitoring the Earth's interior (e.g. Sabra *et al.* 2005; Shapiro *et al.* 2005; Brenguier *et al.* 2008; Duputel *et al.* 2009; Saygin & Kennett 2012; de Ridder *et al.* 2014). The method rests on the assumption that the seismic wavefield is equipartitioned or that the noise sources are homogeneously distributed. Under these conditions, the correlation function can be related to the interstation Green function that carries information on Earth structure (e.g. Lobkis & Weaver 2001; Malcolm *et al.* 2004; Wapenaar 2004; Weaver & Lobkis 2004; Wapenaar & Fokkema 2006; Tromp *et al.* 2010; Tsai 2010).

The effects arising from the failure to meet these conditions have many facets. They include biases in traveltime measurements (Tsai 2009; Froment *et al.* 2010; Fichtner 2014), amplitude errors (Cupillard & Capdeville 2010; Tsai 2011), spurious arrivals and waveform distortions (Halliday & Curtis 2008; Kimman & Trampert 2010; Fichtner 2014) and the frequently observed absence of body waves that are present in the true Green function. While some of these effects may be small, they can become relevant in monitoring applications where subtle changes of noise correlations are mapped into changes of subsurface structure.

The dependence of correlation functions on noise source properties already indicates that trade-offs between Earth structure and noise sources exist. Ignoring these trade-offs can lead to less accurate tomographic images and underestimated uncertainties. It follows that ambient noise correlations should ideally be inverted for both noise sources and Earth structure (Hanasoge 2013a)—similar to earthquake tomography where sources and structure must be estimated jointly to obtain useful results.

This paper has two main goals: (i) provide insight into the nature of source-receiver trade-offs in ambient noise correlations and (ii) establish the foundation for future resolution analysis that properly quantifies source-structure trade-offs. Since all inverse problems are

special in terms of their receiver configuration and data, we limit ourselves to general statements concerning the physics and geometry of these trade-offs. In our analysis, we work under the assumption that the solution of an inverse problem has provided us with an optimal Earth model \mathbf{m} and an optimal noise source model \mathbf{s} that minimize a misfit functional χ . In the vicinity of the optimum, χ can be approximated correct to second-order in terms of the Hessian \mathbf{H} ,

$$\chi(\mathbf{m} + \delta\mathbf{m}, \mathbf{s} + \delta\mathbf{s}) = \chi(\mathbf{m}, \mathbf{s}) + \begin{pmatrix} \delta\mathbf{m} \\ \delta\mathbf{s} \end{pmatrix}^T \begin{pmatrix} \mathbf{H}_{mm} & \mathbf{H}_{sm} \\ \mathbf{H}_{sm} & \mathbf{H}_{ss} \end{pmatrix} \begin{pmatrix} \delta\mathbf{m} \\ \delta\mathbf{s} \end{pmatrix}. \quad (1)$$

The off-diagonal elements of the Hessian, \mathbf{H}_{sm} contain the mixed derivatives of the misfit functional, $\delta_s \delta_m \chi$. They describe trade-offs between structural variations $\delta\mathbf{m}$ and noise source variations $\delta\mathbf{s}$, that is, the extent to which one can compensate for the other without changing the misfit χ beyond the measurement uncertainties. Furthermore, \mathbf{H}_{sm} is equal to the change in sensitivity to Earth structure caused by a perturbation in the noise sources.

As a prelude to the computation and analysis of the off-diagonal elements \mathbf{H}_{sm} , we start in Section 2 with a review of noise correlation modelling. This will be followed in Section 3 by a formalism for the computation of sensitivity kernels for Earth structure and noise sources that simplifies the developments of Tromp *et al.* (2010) while leading to identical results. In Section 4, we present the new development of second-order adjoints for ambient noise correlations that allow us to compute the mixed second derivatives of a misfit functional that encodes the trade-offs between Earth structure and ambient noise sources. The emphasis of this section will be on the nature of these trade-offs, including their dependence on frequency and attenuation.

2 NOISE MODELLING AND CORRELATION FIELDS

2.1 General development

To forward model interstation correlations of ambient noise, we adopt the method developed by Woodard (1997) in helioseismology and later adapted to terrestrial seismology by various authors (e.g. Tromp *et al.* 2010; Basini *et al.* 2013; Hanasoge 2013a,b; Fichtner 2014; Nishida 2014). We start with the definition of the frequency-domain Green function $\mathbf{G}_n(\mathbf{x}, \xi)$ with vector components $G_{in}(\mathbf{x}, \xi)$ as the solution of the governing equations when the right-hand side equals a point-localized force at position ξ in n -direction, that is,

$$\mathcal{L}_x \mathbf{G}_n(\mathbf{x}, \xi) = \mathbf{e}_n \delta(\mathbf{x} - \xi). \quad (2)$$

The symbol \mathcal{L}_x denotes a linear forward modelling operator in the frequency domain acting on the spatial variable \mathbf{x} . In the case of a viscoelastic Earth model, eq. (2) may be explicitly written as (e.g. Kennett 2001; Aki & Richards 2002; Fichtner 2010)

$$-\omega^2 \rho G_{in}(\mathbf{x}, \xi) - \partial_j (\Gamma_{ijkl} \partial_k G_{ln}) = \delta_{in} \delta(\mathbf{x} - \xi), \quad (3)$$

with ρ and Γ_{ijkl} denoting mass density and the elastic tensor, respectively. In the frequency domain, the representation theorem is

$$u_i(\mathbf{x}) = \int_{\xi \in \oplus} G_{in}(\mathbf{x}, \xi) N_n(\xi) d\xi, \quad (4)$$

with \oplus the volume of the Earth, u_i the i th component of the seismic displacement field, $G_{in} = (\mathbf{G}_n)_i$ the i th component of the Green function with excitation in n -direction, and N_n the source field of the ambient noise. In the interest of a condensed notation, we omit dependencies on the angular frequency ω whenever this seems reasonable. The frequency-domain correlation between the noise fields $u_i(\mathbf{x}_1)$ and $u_j(\mathbf{x}_2)$ is then

$$\mathcal{C}_{ij}(\mathbf{x}_1, \mathbf{x}_2) = u_i(\mathbf{x}_1) u_j^*(\mathbf{x}_2) = \iint_{\xi_1, \xi_2 \in \oplus} G_{in}(\mathbf{x}_1, \xi_1) N_n(\xi_1) G_{jm}^*(\mathbf{x}_2, \xi_2) N_m^*(\xi_2) d\xi_1 d\xi_2. \quad (5)$$

Taking the expectation of eq. (5) gives

$$C_{ij}(\mathbf{x}_1, \mathbf{x}_2) = \mathbb{E}[\mathcal{C}_{ij}(\mathbf{x}_1, \mathbf{x}_2)] = \iint_{\xi_1, \xi_2 \in \oplus} G_{in}(\mathbf{x}_1, \xi_1) G_{jm}^*(\mathbf{x}_2, \xi_2) \mathbb{E}[N_n(\xi_1) N_m^*(\xi_2)] d\xi_1 d\xi_2. \quad (6)$$

Under the assumption that the noise sources are spatially uncorrelated, in the sense

$$\mathbb{E}[N_n(\xi_1) N_m^*(\xi_2)] = S_{nm}(\xi_1) \delta(\xi_1 - \xi_2), \quad (7)$$

eq. (6) condenses to

$$C_{ij}(\mathbf{x}_1, \mathbf{x}_2) = \int_{\xi \in \oplus} G_{in}(\mathbf{x}_1, \xi) G_{jm}^*(\mathbf{x}_2, \xi) S_{nm}(\xi) d\xi. \quad (8)$$

The power-spectral density distribution S_{nm} satisfies the relation $S_{nm} = S_{mn}^*$. It may be estimated from ocean wave models (Ardhuin *et al.* 2011) or the inversion of ambient noise data (Nishida & Fukao 2007; Nishida 2014). In practice, the expectation $C_{ij} = \mathbb{E}[\mathcal{C}_{ij}]$ cannot be computed because there is only one realization of the global noise field. Instead, the expectation is commonly replaced by a time average or

temporal stack over correlation windows of a pre-defined length (e.g. Bensen *et al.* 2007; Groos *et al.* 2012). As pointed out by Snieder *et al.* (2010), the time average approximates the expectation because dissipation effectively resets the clock after a characteristic decay time so that consecutive wavefield samples are practically independent.

The interstation correlation C_{ij} for variable components i and j can be interpreted as a tensor quantity,

$$\mathbf{C}(\mathbf{x}_1, \mathbf{x}_2) = \int_{\xi \in \oplus} \mathbf{G}_n(\mathbf{x}_1, \xi) \otimes \mathbf{G}_m^*(\mathbf{x}_2, \xi) S_{nm}(\xi) d\xi, \quad (9)$$

where \otimes denotes the tensor or dyadic product. Individual components of the correlation can be retrieved via products with the unit vectors \mathbf{e}_i and \mathbf{e}_j , that is $C_{ij} = \mathbf{e}_i \cdot \mathbf{C} \cdot \mathbf{e}_j$. Furthermore, the Hermitian transpose of \mathbf{C} satisfies the symmetry relation $\mathbf{C}^H(\mathbf{x}_1, \mathbf{x}_2) = \mathbf{C}(\mathbf{x}_2, \mathbf{x}_1)$. Based on eq. (9), we see that the vector field

$$\mathbf{C}_{\cdot j}(\mathbf{x}, \mathbf{x}_2) = \mathbf{C}(\mathbf{x}, \mathbf{x}_2) \cdot \mathbf{e}_j = \int_{\xi \in \oplus} \mathbf{G}_n(\mathbf{x}, \xi) [S_{nm}(\xi) G_{jm}^*(\mathbf{x}_2, \xi)] d\xi \quad (10)$$

is a solution of the wave equation. This ‘correlation wavefield’ is excited by the deterministic source $f_n(\xi) = S_{nm}(\xi) G_{mj}^*(\xi, \mathbf{x}_2)$. Similarly, the correlation wavefield $\mathbf{C}_{\cdot i}^H(\mathbf{x}_1, \mathbf{x}) = \mathbf{C}^H(\mathbf{x}_1, \mathbf{x}) \cdot \mathbf{e}_i$ is excited by the source $f_n(\xi) = S_{nm}(\xi) G_{mi}^*(\xi, \mathbf{x}_1)$. Eq. (10) suggests a numerical recipe for the computation of correlation functions for which the reference receiver is located at position \mathbf{x}_2 : First, the Green function with source at \mathbf{x}_2 is computed, and its complex conjugate is multiplied with the power-spectral density S_{nm} to yield the source of the correlation wavefield. Second, the correlation wavefield is computed as regular solution to the wave equation using the previously constructed source. Finally, the correlation wavefield is sampled at any position where another receiver is located.

In our development, we have not made any assumption on the nature of the noise sources. They may be ocean waves and atmospheric turbulences coupling with the solid Earth (e.g. Nishida & Fukao 2007; Arduin *et al.* 2011; Gaultier *et al.* 2013; Nishida 2014), or small-scale scatterers that excite secondary wavefields and coda (e.g. Snieder 2004; Planes *et al.* 2015).

2.2 Examples in a 2-D acoustic, attenuating medium

While the development in Section 3.1.1 is general and valid for any viscoelastic wavefield in 3-D, we will use a 2-D homogeneous, acoustic and attenuating medium for the purpose of illustration. Especially the analysis of source-structure trade-offs in Section 4 will greatly benefit from this simplification, even though it neglects some aspects of wave propagation in the 3-D Earth. We specifically consider the frequency-domain wave equation operator \mathcal{L} defined by

$$\mathcal{L}u = -\omega^2 \rho u - \partial_x(\mu \partial_x u), \quad (11)$$

where the shear modulus μ is allowed to be frequency-dependent to incorporate viscoelastic dissipation. The far-field Green function of \mathcal{L} is given by

$$G(\mathbf{x}, \xi, \omega) = -i \frac{1}{4\rho v^2} \sqrt{\frac{2v}{\pi \omega r}} e^{-i \frac{\omega}{v} r} e^{-\frac{\omega r}{2vQ}} e^{i \frac{\pi}{4}}, \quad (12)$$

with the phase velocity $v = \sqrt{\mu/\rho}$, the source-receiver distance $r = |\mathbf{x} - \xi|$, and the quality factor Q (Bath 1968). Adopting eq. (8) for the interstation correlation function to the acoustic case, gives

$$C(\mathbf{x}_1, \mathbf{x}_2) = \int_{\xi \in \oplus} G(\mathbf{x}_1, \xi) G^*(\mathbf{x}_2, \xi) S(\xi) d\xi, \quad (13)$$

which we can evaluate analytically using the Green function from eq. (12). Fig. 1 shows examples of time-domain correlation functions in an 8×10^6 m by 4×10^6 m wide domain, with $v = 3000$ m s $^{-1}$, $\rho = 3000$ kg m $^{-3}$ and Q taking the values 50, 200 and ∞ . The correlation functions are bandpass filtered between 10 and 30 mHz.

As expected, correlation functions are perfectly symmetric in the case of a homogeneous noise source distribution, shown in the left column of Fig. 1. When noise sources are confined to the upper-right quarter of the spatial domain, the symmetry is broken, the acausal part of the correlation function vanishes and a spurious antisymmetric waveform appears around $t = 0$.

3 FIRST-ORDER ADJOINTS: FRÉCHET KERNELS

Following the computation of synthetic correlation functions $C_{ij}(\mathbf{x}_1, \mathbf{x}_2)$, we can perform measurements to quantify their deviation from observed correlation functions $C_{ij}^0(\mathbf{x}_1, \mathbf{x}_2)$. We denote the measurement or misfit functional by χ . In Appendix A, we show that the variation of χ with respect to perturbations in Earth structure or noise source distribution can generally be written as

$$\delta\chi = 2 \operatorname{Re} \int_{\omega=0}^{\infty} \delta C_{ij}(\mathbf{x}_1, \mathbf{x}_2, \omega) f(\omega) d\omega. \quad (14)$$

In eq. (14), δC_{ij} denotes the variation of the synthetic correlation function, and f will later play the role of an adjoint source.

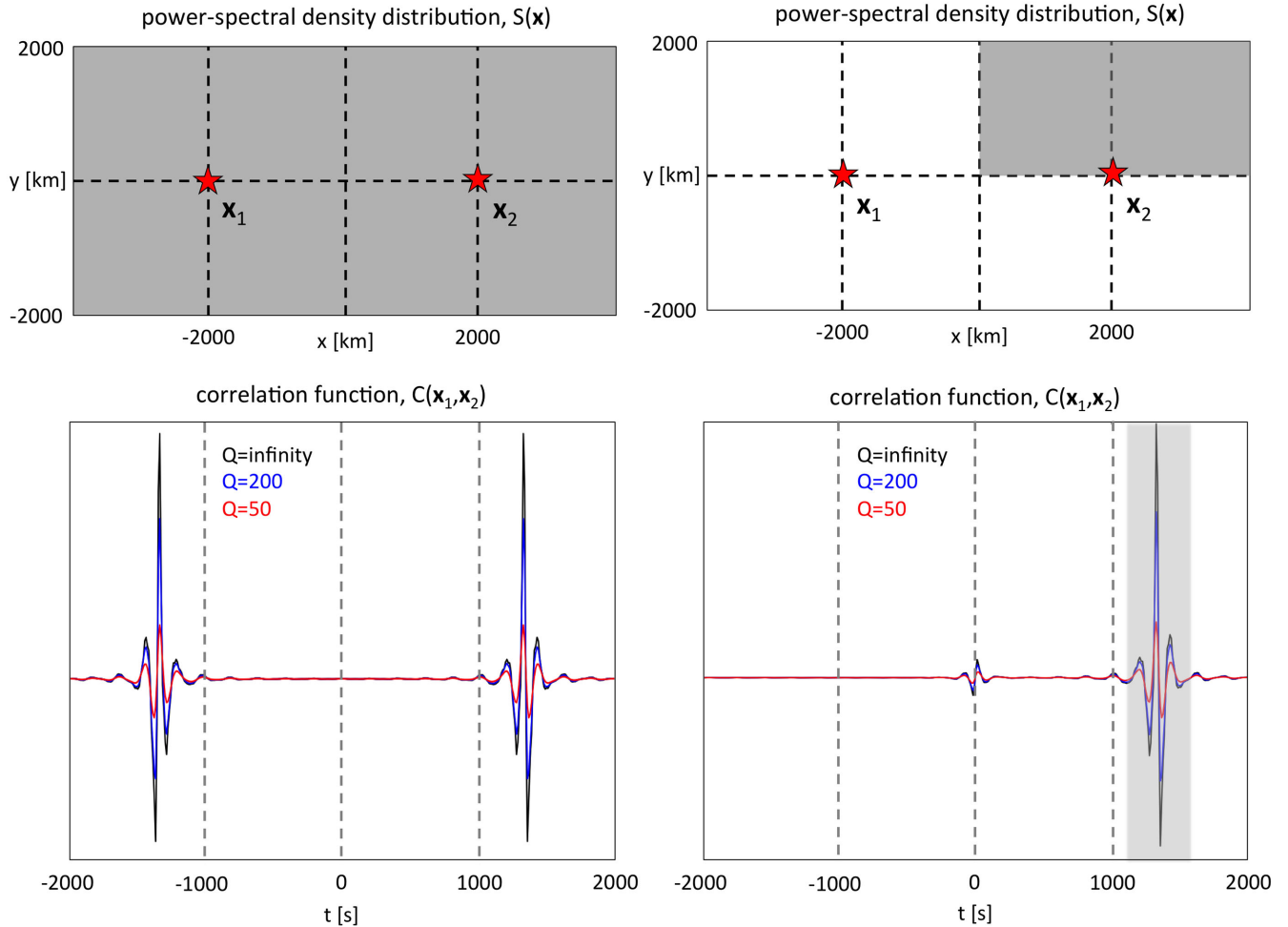


Figure 1. Distributions of the noise source power-spectral density $S(\mathbf{x})$ (top) and the resulting interstation correlation functions $C(\mathbf{x}_1, \mathbf{x}_2)$ for different Q values (bottom). Grey-shaded areas in the power-spectral density distributions correspond to $S(\mathbf{x}) = 1$, whereas white corresponds to $S(\mathbf{x}) = 0$. The positions of the receivers are indicated by red stars. For a homogeneous source distribution (left), the correlation functions are perfectly symmetric. When noise sources are confined to the upper-right quarter of the domain, the acausal part of the correlation function vanishes as expected, and an antisymmetric contribution appears around $t = 0$. Light grey shading in the lower right panel indicates the measurement interval used for the computation of sensitivity kernels in the following sections. See the text for details on medium properties and frequency content.

3.1 Kernels for noise source distribution

3.1.1 General development

For variations in the noise source distribution, δS_{nm} , the variation of the synthetic correlation function takes the specific form

$$\delta C_{ij}(\mathbf{x}_1, \mathbf{x}_2) = \int_{\mathbf{x} \in \oplus} G_{in}(\mathbf{x}_1, \mathbf{x}) \delta S_{nm}(\mathbf{x}) G_{jm}^*(\mathbf{x}_2, \mathbf{x}) d\mathbf{x}. \quad (15)$$

Inserting eq. (15) into eq. (14) we obtain

$$\delta \chi = 2 \int_{\omega=0}^{\infty} \int_{\mathbf{x} \in \oplus} f G_{in}(\mathbf{x}_1, \mathbf{x}) \delta S_{nm}(\mathbf{x}) G_{jm}^*(\mathbf{x}_2, \mathbf{x}) d\omega d\mathbf{x} = \int_{\omega=0}^{\infty} \int_{\mathbf{x} \in \oplus} K_{nm}(\mathbf{x}, \omega) \delta S_{nm}(\mathbf{x}, \omega) d\mathbf{x} d\omega, \quad (16)$$

with the space- and frequency-dependent noise source kernels given by

$$K_{nm}(\mathbf{x}, \omega) = 2 f(\omega) G_{in}(\mathbf{x}_1, \mathbf{x}, \omega) G_{jm}^*(\mathbf{x}_2, \mathbf{x}, \omega). \quad (17)$$

In eq. (17), the adjoint source f acts merely as a scalar weighting factor for kernels at different frequencies—the geometry of which is entirely determined by the Green functions emitted from the two receiver positions. In this context, it is important to note that ω in eq. (17) is not the frequency at which measurements are performed but the frequency at which the sensitivity to the noise source distribution is considered. The meaning of ω becomes more apparent when the frequency dependence of the power-spectral density S_{nm} is discretized, as

it would be in a realistic inverse problem where a continuous and infinite-dimensional frequency dependence cannot be resolved. Adopting the parametrization with piecewise constant basis functions $h^\ell(\omega)$

$$S_{nm}(\mathbf{x}, \omega) = \sum_\ell s_{nm}^\ell(\mathbf{x}) h^\ell(\omega), \quad h^\ell(\omega) = \begin{cases} (\omega_{\ell+1} - \omega_\ell)^{-1}, & \omega \in [\omega_\ell, \omega_{\ell+1}] \\ 0, & \text{otherwise} \end{cases}, \quad (18)$$

we find

$$\delta\chi = \sum_\ell \int_{\mathbf{x} \in \oplus} K_{nm}^\ell(\mathbf{x}) \delta s_{nm}^\ell(\mathbf{x}), \quad (19)$$

where the *finite-band* source kernels $K_{nm}^\ell(\mathbf{x})$ are computed from the *monochromatic* source kernels $K_{nm}(\mathbf{x})$ via the integration

$$K_{nm}^\ell(\mathbf{x}) = \int_{\omega=\omega_\ell}^{\omega_{\ell+1}} K_{nm}(\omega, \mathbf{x}) d\omega. \quad (20)$$

The integration over frequency will generally de-emphasize rapid oscillations in the kernels, leading to broader-scale features. This is illustrated in the following section where we return to the simplified 2-D acoustic medium.

3.1.2 Examples in a 2-D acoustic, attenuating medium

Using again the acoustic model from Section 2.2, we can compute noise source kernels with scalar versions of eqs (17) and (20):

$$K(\mathbf{x}, \omega) = 2 f(\omega) G(\mathbf{x}_1, \mathbf{x}, \omega) G^*(\mathbf{x}_2, \mathbf{x}, \omega), \quad K^\ell(\mathbf{x}) = \int_{\omega=\omega_\ell}^{\omega_{\ell+1}} K(\omega, \mathbf{x}) d\omega. \quad (21)$$

As measurement, we choose cross-correlation traveltimes (Luo & Schuster 1991) performed on the causal part of the correlation function computed for the noise sources confined to the upper-right quarter of the spatial domain. The measurement interval is marked grey in Fig. 1. In Appendix A, we show that the frequency-domain adjoint source f for the traveltime measurement is given by

$$f(\omega) = -i \frac{\omega C^*(\mathbf{x}_1, \mathbf{x}_2)}{\int \omega^2 |C|^2 d\omega}. \quad (22)$$

In the acoustic model, the structure kernel $K(\mathbf{x}, \omega)$ is a product of complex exponentials, with phase $\phi(\mathbf{x}, \omega)$ approximately given by

$$\phi(\mathbf{x}, \omega) \approx \frac{i\omega}{v} \left(\underbrace{|\mathbf{x}_1 - \mathbf{x}_2|}_{\text{from } f} - \underbrace{|\mathbf{x}_1 - \mathbf{x}|}_{\text{from } G(\mathbf{x}_1, \mathbf{x})} + \underbrace{|\mathbf{x}_2 - \mathbf{x}|}_{\text{from } G^*(\mathbf{x}_2, \mathbf{x})} \right). \quad (23)$$

The regions of constant phase are hyperbolas with foci near \mathbf{x}_1 and \mathbf{x}_2 that can be seen in the narrow-band kernels (0.020–0.021 Hz) of Fig. 2 (bottom). The integral over frequency in eq. (22) suppresses contributions outside the stationary-phase region where $\phi(\mathbf{x}, \omega) \approx 0$. Consequently, the broad-band kernels (0.01–0.03 Hz) in Fig. 2 (top) only feature hyperbolic jets extending from the receiver at \mathbf{x}_2 towards the right. This structure is consistent with the intuitive expectation that only noise originating from behind the receiver at \mathbf{x}_2 and passing through both \mathbf{x}_2 and \mathbf{x}_1 should affect the causal part of the correlation function $C(\mathbf{x}_1, \mathbf{x}_2)$. The effect of Q manifests itself mostly in the decay of sensitivity with increasing distance from the receivers. For low Q , sensitivity decays quickly, indicating that only noise sources in the vicinity of the receivers can perturb the measurement.

Most of the described features, including the hyperbolic jets and the Q -related decay, are independent of the measurement. Exchanging measurements on the causal part for measurements on the acausal part, would mirror the sensitivity distribution with respect to the $x = 0$ axis.

3.2 Kernels for Earth structure

3.2.1 General development

To derive sensitivity kernels for variations in Earth structure, we depart again from the general expression (14) for the variation of the misfit or measurement functional that we repeat here for convenience:

$$\delta\chi = 2 \operatorname{Re} \int_{\omega=0}^{\infty} \delta C_{ij}(\mathbf{x}_1, \mathbf{x}_2, \omega) f(\omega) d\omega. \quad (24)$$

Again, the specific form of $f(\omega)$ depends on the particular definition of χ . Introducing into eq. (24) the first variation of $C_{ij}(\mathbf{x}_1, \mathbf{x}_2, \omega)$ with respect to Earth model parameters,

$$\delta C_{ij}(\mathbf{x}_1, \mathbf{x}_2) = \int_{\xi \in \oplus} G_{in}(\mathbf{x}_1, \xi) \delta G_{jm}^*(\mathbf{x}_2, \xi) S_{nm}(\xi) d\xi + \int_{\xi \in \oplus} \delta G_{in}(\mathbf{x}_1, \xi) G_{jm}^*(\mathbf{x}_2, \xi) S_{nm}(\xi) d\xi, \quad (25)$$

gives the first variation of χ in terms of the first variations of Green functions:

$$\delta\chi = 2 \operatorname{Re} \int_{\omega=0}^{\infty} \int_{\xi \in \oplus} G_{in}(\mathbf{x}_1, \xi) \delta G_{jm}^*(\mathbf{x}_2, \xi) S_{nm}(\xi) f d\xi d\omega + 2 \operatorname{Re} \int_{\omega=0}^{\infty} \int_{\xi \in \oplus} \delta G_{in}(\mathbf{x}_1, \xi) G_{jm}^*(\mathbf{x}_2, \xi) S_{nm}(\xi) f d\xi d\omega. \quad (26)$$

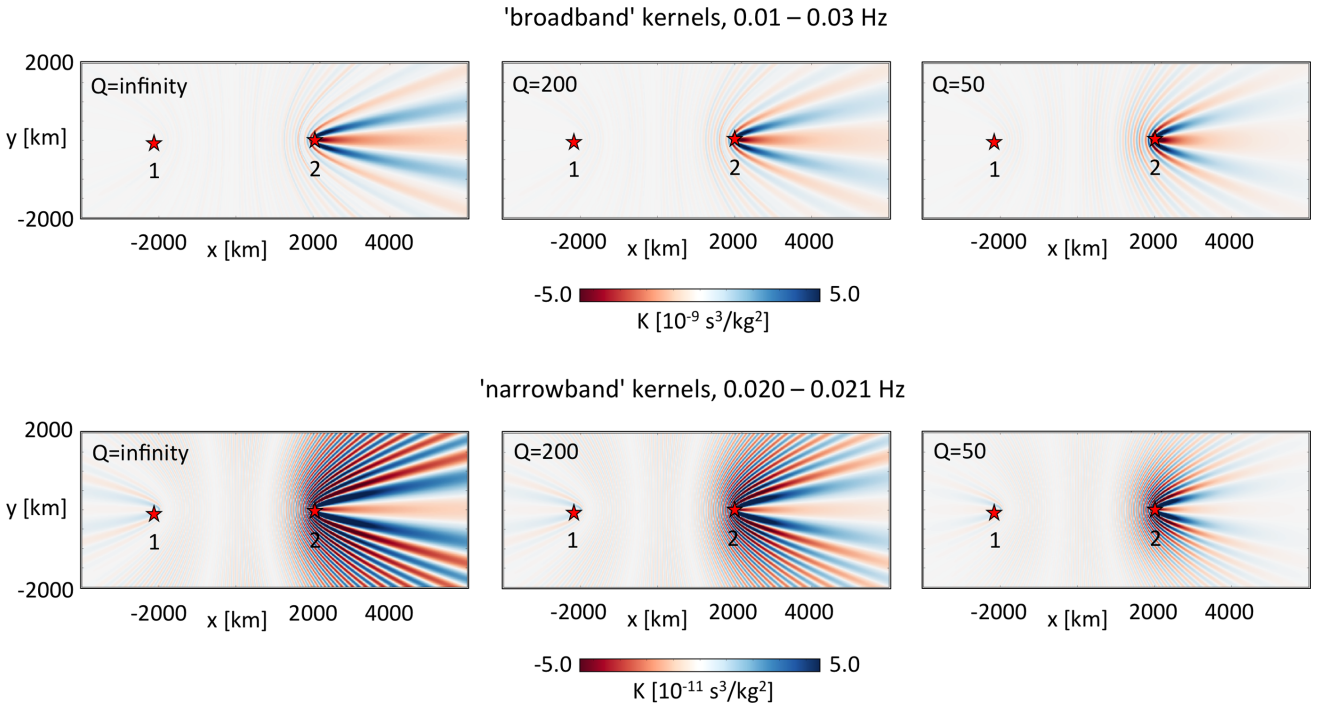


Figure 2. Noise source kernels for cross-correlation traveltimes measurements on the causal part of the correlation functions displayed in Fig. 1 for different values of Q . Kernels for a broader frequency band from 0.01 to 0.03 Hz are displayed in the top row, and kernels for a narrow frequency band from 0.020 to 0.021 Hz are displayed in the bottom row.

With the help of Green's theorem (see Appendix B)

$$\delta G_{ij}(\mathbf{x}_1, \xi) = - \int_{\mathbf{x} \in \oplus} \mathbf{G}_i^\dagger(\mathbf{x}, \mathbf{x}_1) \cdot [\delta \mathcal{L}_x \mathbf{G}_j(\mathbf{x}, \xi)] d\mathbf{x}, \quad (27)$$

we can replace the first variations of Green functions in (26) by products of forward and adjoint Green functions:

$$\begin{aligned} \delta \chi = & -2 \operatorname{Re} \int_{\omega=0}^{\infty} \int_{\xi \in \oplus} \int_{\mathbf{x} \in \oplus} G_{in}(\mathbf{x}_1, \xi) G_{kj}^*(\mathbf{x}, \mathbf{x}_2) [\delta \mathcal{L}_x^* \mathbf{G}_m^*(\mathbf{x}, \xi)]_k S_{nm}(\xi) f d\mathbf{x} d\xi d\omega . \\ & -2 \operatorname{Re} \int_{\omega=0}^{\infty} \int_{\xi \in \oplus} \int_{\mathbf{x} \in \oplus} G_{ki}^\dagger(\mathbf{x}, \mathbf{x}_1) G_{jm}^*(\mathbf{x}_2, \xi) [\delta \mathcal{L}_x \mathbf{G}_n(\mathbf{x}, \xi)]_k S_{nm}(\xi) f d\mathbf{x} d\xi d\omega . \end{aligned} \quad (28)$$

Rearranging terms in eq. (28) such that the adjoint Green functions appear first under the triple integrals yields

$$\begin{aligned} \delta \chi = & -2 \operatorname{Re} \int_{\omega=0}^{\infty} \int_{\mathbf{x} \in \oplus} G_{kj}^*(\mathbf{x}, \mathbf{x}_2) f \left[\delta \mathcal{L}_x^* \int_{\xi \in \oplus} \mathbf{G}_m^*(\mathbf{x}, \xi) G_{in}(\mathbf{x}_1, \xi) S_{nm}(\xi) d\xi \right]_k d\mathbf{x} d\omega \\ & -2 \operatorname{Re} \int_{\omega=0}^{\infty} \int_{\mathbf{x} \in \oplus} G_{ki}^\dagger(\mathbf{x}, \mathbf{x}_1) f \left[\delta \mathcal{L}_x \int_{\xi \in \oplus} \mathbf{G}_n(\mathbf{x}, \xi) G_{jm}^*(\mathbf{x}_2, \xi) S_{nm}(\xi) d\xi \right]_k d\mathbf{x} d\omega . \end{aligned} \quad (29)$$

With the help of the correlation wavefields defined in eq. (10), we can condense eq. (29) to

$$\delta \chi = -2 \operatorname{Re} \int_{\omega=0}^{\infty} \int_{\mathbf{x} \in \oplus} G_{kj}^\dagger(\mathbf{x}, \mathbf{x}_2) f^* [\delta \mathcal{L}_x \mathbf{C}_{.i}(\mathbf{x}, \mathbf{x}_1)]_k d\mathbf{x} d\omega - 2 \operatorname{Re} \int_{\omega=0}^{\infty} \int_{\mathbf{x} \in \oplus} G_{ki}^\dagger(\mathbf{x}, \mathbf{x}_1) f [\delta \mathcal{L}_x \mathbf{C}_{.j}(\mathbf{x}, \mathbf{x}_2)]_k d\mathbf{x} d\omega . \quad (30)$$

Furthermore, defining the adjoint fields

$$\mathbf{u}_j^{(2)}(\mathbf{x}) = \mathbf{G}_j^\dagger(\mathbf{x}, \mathbf{x}_2) f^* \quad \text{and} \quad \mathbf{u}_i^{(1)}(\mathbf{x}) = \mathbf{G}_i^\dagger(\mathbf{x}, \mathbf{x}_1) f , \quad (31)$$

respectively, we obtain

$$\delta \chi = -2 \operatorname{Re} \int_{\omega=0}^{\infty} \int_{\mathbf{x} \in \oplus} \mathbf{u}_j^{(2)}(\mathbf{x}) \cdot [\delta \mathcal{L}_x \mathbf{C}_{.i}(\mathbf{x}, \mathbf{x}_1)] d\mathbf{x} d\omega - 2 \operatorname{Re} \int_{\omega=0}^{\infty} \int_{\mathbf{x} \in \oplus} \mathbf{u}_i^{(1)}(\mathbf{x}) \cdot [\delta \mathcal{L}_x \mathbf{C}_{.j}(\mathbf{x}, \mathbf{x}_2)] d\mathbf{x} d\omega . \quad (32)$$

The structure of eq. (32) is similar to the structure of $\delta \chi$ when a traditional source-receiver configuration is used (e.g. Tarantola 1988; Tromp *et al.* 2005; Fichtner *et al.* 2006; Chen 2011). The variation is given by a product of a forward field and an adjoint field, integrated over space and frequency—or over time, when working in the time domain. Correlation fields emanating from the receiver positions \mathbf{x}_1 and \mathbf{x}_2 , respectively, play the roles of the forward field. The correlation field emitted from \mathbf{x}_1 interacts with the adjoint field $\mathbf{u}_j^{(2)}$ emitted from \mathbf{x}_2 , and vice versa.

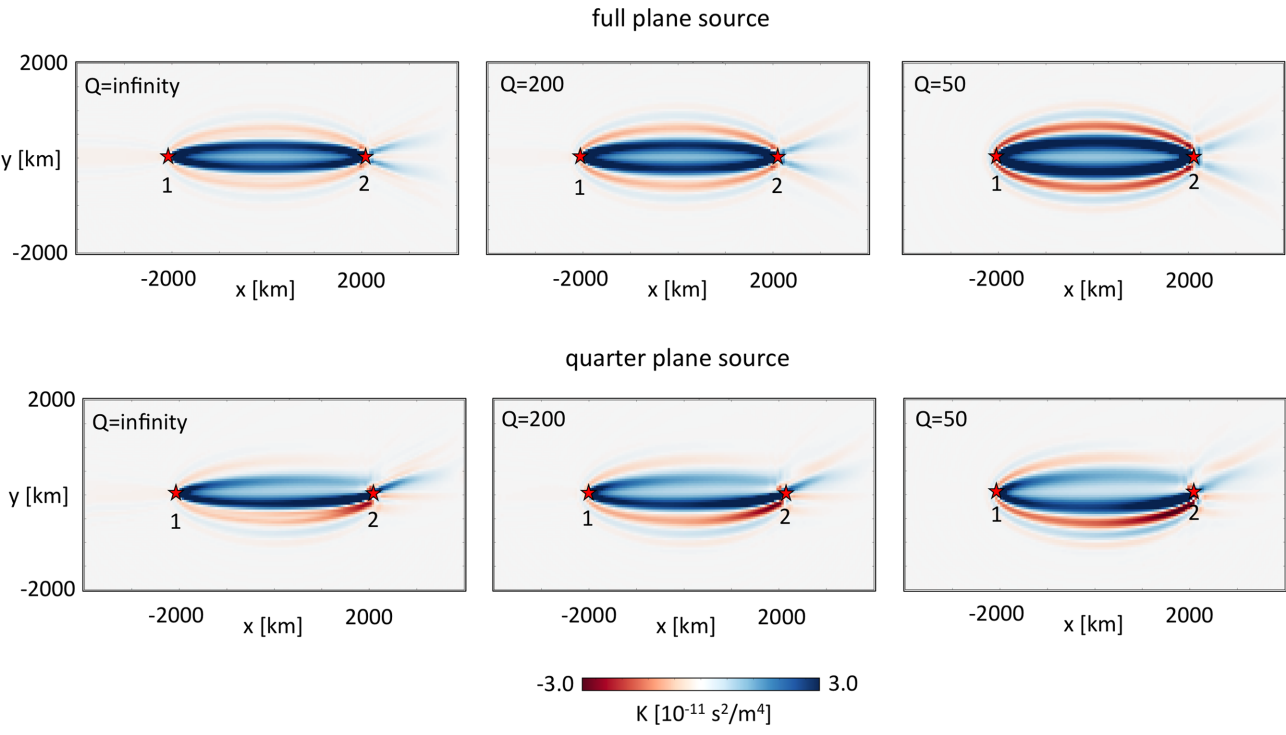


Figure 3. Sensitivity kernels for 2-D velocity structure as a function of Q . Kernels for a noise source $S(\mathbf{x})$ distributed homogeneously across the domain are shown in the top row. The bottom row shows kernels for noise source restricted to the upper-right quarter plane. See also Fig. 1 for the noise source geometry.

The specific form of eq. (32) depends on the forward modelling operator \mathcal{L} and the model parameters that are perturbed. Using the viscoelastic wave equation operator from eq. (3), the variation with respect to density, δ_ρ , is given by

$$\delta_\rho \chi = 2 \operatorname{Re} \int_{\omega=0}^{\infty} \int_{\mathbf{x} \in \oplus} \omega^2 \mathbf{u}_j^{(2)}(\mathbf{x}) \cdot \mathbf{C}_{\cdot i}(\mathbf{x}, \mathbf{x}_1) \delta\rho(\mathbf{x}) d\mathbf{x} d\omega + 2 \operatorname{Re} \int_{\omega=0}^{\infty} \int_{\mathbf{x} \in \oplus} \omega^2 \mathbf{u}_i^{(1)}(\mathbf{x}) \cdot \mathbf{C}_{\cdot j}(\mathbf{x}, \mathbf{x}_2) \delta\rho(\mathbf{x}) d\mathbf{x} d\omega. \quad (33)$$

Defining the sensitivity kernel $K_\rho(\mathbf{x})$ as

$$K_\rho(\mathbf{x}) = 2 \operatorname{Re} \int_{\omega=0}^{\infty} \omega^2 \mathbf{u}_j^{(2)}(\mathbf{x}) \cdot \mathbf{C}_{\cdot i}(\mathbf{x}, \mathbf{x}_1) d\omega + 2 \operatorname{Re} \int_{\omega=0}^{\infty} \omega^2 \mathbf{u}_i^{(1)}(\mathbf{x}) \cdot \mathbf{C}_{\cdot j}(\mathbf{x}, \mathbf{x}_2) d\omega, \quad (34)$$

allows us to condense eq. (33) into

$$\delta_\rho \chi = \int_{\mathbf{x} \in \oplus} K_\rho(\mathbf{x}) \delta\rho(\mathbf{x}) d\mathbf{x}. \quad (35)$$

Following the same recipe, similar kernels can be derived for variations in elastic parameters, seismic velocities or parameters describing attenuation (Fichtner 2010).

3.2.2 Examples in a 2-D acoustic, attenuating medium

In the acoustic case, the vectorial expression (32) simplifies to the scalar expression

$$\delta\chi = -2 \operatorname{Re} \int_{\omega=0}^{\infty} \int_{\mathbf{x} \in \oplus} \underbrace{u^{(2)}(\mathbf{x}) [\delta\mathcal{L}_x C(\mathbf{x}, \mathbf{x}_1)]}_{\text{I}} d\mathbf{x} d\omega - 2 \operatorname{Re} \int_{\omega=0}^{\infty} \int_{\mathbf{x} \in \oplus} \underbrace{u^{(1)}(\mathbf{x}) [\delta\mathcal{L}_x C(\mathbf{x}, \mathbf{x}_2)]}_{\text{II}} d\mathbf{x} d\omega. \quad (36)$$

As for the source kernels, significant contributions to the kernels only appear in the stationary-phase regions of the integrands I and II of eq. (36). Using again the traveltime measurement in the causal part of the correlation function—already employed for the computation of source kernels in Section 3.1.2—we find that the phase of the adjoint field $u^{(2)}$ is approximately given by $\frac{i\omega}{v}(|\mathbf{x}_1 - \mathbf{x}_2| - |\mathbf{x} - \mathbf{x}_1|)$. The phase of the correlation wavefield $C(\mathbf{x}, \mathbf{x}_1)$ generally depends on the noise source distribution $S(\mathbf{x})$. Provided that $S(\mathbf{x})$ is sufficiently homogeneous, the phase of $C(\mathbf{x}, \mathbf{x}_1)$ is close to the phase of a wave propagating from a point source at \mathbf{x}_1 to some position \mathbf{x} , that is $-\frac{i\omega}{v}(|\mathbf{x} - \mathbf{x}_1|)$. In summary, the stationary-phase region of the integrand I in eq. (36) is approximated by

$$|\mathbf{x} - \mathbf{x}_1| + |\mathbf{x} - \mathbf{x}_2| \approx |\mathbf{x}_1 - \mathbf{x}_2|, \quad (37)$$

which defines an ellipsoid around the line connecting \mathbf{x}_1 and \mathbf{x}_2 . For the stationary-phase region of integrand II we find the same expression, meaning that the complete sensitivity kernel should have elliptical geometry. This is confirmed by the numerical examples shown in Fig. 3.

Departures from symmetry and a purely elliptical shape are mostly related to the noise source distribution (e.g. Tromp *et al.* 2010; Nishida 2011). The finiteness of the computational domain, and thus the finite domain covered with noise sources, results in a faint tail behind receiver \mathbf{x}_2 , even when the source distribution within the domain is homogeneous. This tail is similar to the one found in finite-frequency kernel two-station measurements on earthquake data (de Vos *et al.* 2013). Covering only a quarter of the domain with noise sources breaks the symmetry of kernels because the stationary-phase region is no longer described adequately by relation (37) where \mathbf{x}_1 and \mathbf{x}_2 can be interchanged. Attenuation manifests itself in a broadening of the kernels as Q decreases. High attenuation eliminates the higher-frequency components of the Green functions that are more concentrated around the receiver-receiver line. Thus, lower-frequency components with broader Fresnel zones gain dominance.

4 MIXED DERIVATIVES AND SOURCE-STRUCTURE TRADE-OFFS

With the formalism introduced in Sections 2 and 3, we can derive mixed second derivatives of the measurement functional χ . The mixed derivatives provide information on trade-offs between Earth structure and noise sources, and on the extent to which kernels for structure change when noise sources are perturbed, and vice versa.

4.1 Derivation of mixed source-structure derivatives

We start the derivation of mixed derivatives with a slight modification of the previously employed notation. From now on, we denote by δ_m variations with respect to Earth structure, and by δ_s variations with respect to the noise source distribution. With this convention, the variation of χ with respect to Earth structure given in eq. (29) takes the form

$$\begin{aligned} \delta_m \chi = & -2 \operatorname{Re} \int_{\omega=0}^{\infty} \int_{\mathbf{x} \in \oplus} G_{kj}^{\dagger}(\mathbf{x}, \mathbf{x}_2) f^* \left[\delta_m \mathcal{L}_x \int_{\xi \in \oplus} \mathbf{G}_m(\mathbf{x}, \xi) G_{in}^*(\mathbf{x}_1, \xi) S_{mn}(\xi) d\xi \right]_k d\mathbf{x} d\omega \\ & -2 \operatorname{Re} \int_{\omega=0}^{\infty} \int_{\mathbf{x} \in \oplus} G_{ki}^{\dagger}(\mathbf{x}, \mathbf{x}_1) f \left[\delta_m \mathcal{L}_x \int_{\xi \in \oplus} \mathbf{G}_n(\mathbf{x}, \xi) G_{jm}^*(\mathbf{x}_2, \xi) S_{nm}(\xi) d\xi \right]_k d\mathbf{x} d\omega. \end{aligned} \quad (38)$$

In addition to the explicit dependence of $\delta_m \chi$ on S_{nm} , there is an implicit dependence on S_{nm} hidden in the adjoint source f because the measurement changes in response to a perturbation of the noise source distribution. Taking both explicit and implicit dependences into account, the mixed variation $\delta_s \delta_m \chi$ is given by

$$\begin{aligned} \delta_s \delta_m \chi = & -2 \operatorname{Re} \int_{\omega=0}^{\infty} \int_{\mathbf{x} \in \oplus} \underbrace{G_{kj}^{\dagger}(\mathbf{x}, \mathbf{x}_2) f^*}_{u_{kj}^2(\mathbf{x})} \left[\delta_m \mathcal{L}_x \underbrace{\int_{\xi \in \oplus} \mathbf{G}_m(\mathbf{x}, \xi) G_{in}^*(\mathbf{x}_1, \xi) \delta S_{mn}(\xi) d\xi}_{\delta_s \mathbf{C}_{..i}(\mathbf{x}, \mathbf{x}_1)} \right]_k d\mathbf{x} d\omega \\ & -2 \operatorname{Re} \int_{\omega=0}^{\infty} \int_{\mathbf{x} \in \oplus} \underbrace{G_{ki}^{\dagger}(\mathbf{x}, \mathbf{x}_1) f}_{u_{ki}^1(\mathbf{x})} \left[\delta_m \mathcal{L}_x \underbrace{\int_{\xi \in \oplus} \mathbf{G}_n(\mathbf{x}, \xi) G_{jm}^*(\mathbf{x}_2, \xi) \delta S_{nm}(\xi) d\xi}_{\delta_s \mathbf{C}_{..j}(\mathbf{x}, \mathbf{x}_2)} \right]_k d\mathbf{x} d\omega \\ & -2 \operatorname{Re} \int_{\omega=0}^{\infty} \int_{\mathbf{x} \in \oplus} \underbrace{G_{kj}^{\dagger}(\mathbf{x}, \mathbf{x}_2) \delta_s f^*}_{\delta_s u_{kj}^2(\mathbf{x})} \left[\delta_m \mathcal{L}_x \underbrace{\int_{\xi \in \oplus} \mathbf{G}_m(\mathbf{x}, \xi) G_{in}^*(\mathbf{x}_1, \xi) S_{mn}(\xi) d\xi}_{\mathbf{C}_{..i}(\mathbf{x}, \mathbf{x}_1)} \right]_k d\mathbf{x} d\omega \\ & -2 \operatorname{Re} \int_{\omega=0}^{\infty} \int_{\mathbf{x} \in \oplus} \underbrace{G_{ki}^{\dagger}(\mathbf{x}, \mathbf{x}_1) \delta_s f}_{\delta_s u_{ki}^1(\mathbf{x})} \left[\delta_m \mathcal{L}_x \underbrace{\int_{\xi \in \oplus} \mathbf{G}_n(\mathbf{x}, \xi) G_{jm}^*(\mathbf{x}_2, \xi) S_{nm}(\xi) d\xi}_{\mathbf{C}_{..j}(\mathbf{x}, \mathbf{x}_2)} \right]_k d\mathbf{x} d\omega. \end{aligned} \quad (39)$$

As indicated by the underbraces, this complicated expression may be simplified using variations of the forward correlation fields $\mathbf{C}(\mathbf{x}, \mathbf{x}_1)$, $\mathbf{C}(\mathbf{x}, \mathbf{x}_2)$ and the adjoint fields $u_{ki}^1(\mathbf{x}), u_{kj}^2(\mathbf{x})$. In analogy to eq. (33), we may write eq. (38) in terms of volumetric sensitivity kernels:

$$\delta_s \delta_m \chi = \int_{\mathbf{x} \in \oplus} \delta_f K_{ij} \delta \mathbf{m} d\mathbf{x} + \int_{\mathbf{x} \in \oplus} \delta_c K_{ij} \delta \mathbf{m} d\mathbf{x}. \quad (40)$$

The ‘trade-off kernel’ $\delta_c K_{ij}$ is computed just as K_{ij} , but with the forward correlation fields $\mathbf{C}(\mathbf{x}, \mathbf{x}_1)$ and $\mathbf{C}(\mathbf{x}, \mathbf{x}_2)$ replaced by their variations $\delta_s \mathbf{C}(\mathbf{x}, \mathbf{x}_1)$ and $\delta_s \mathbf{C}(\mathbf{x}, \mathbf{x}_2)$, respectively. Similarly, the trade-off kernel $\delta_f K_{ij}$ is computed as K_{ij} where the adjoint source f is replaced by its variation $\delta_s f$.

4.2 Contributions to source-structure trade-offs

Eqs (39) and (40) reveal that the mixed variation $\delta_s \delta_m \chi$ has two types of contributions, corresponding to different aspects of wave propagation physics.

First, the sensitivity to Earth structure $\delta_m \chi$ changes in response to perturbations of the source distribution because it directly affects the measurement. A noise source perturbation δS_{nm} located within the non-zero region of the noise source kernel changes the measurement from χ to $\chi + \delta_s \chi$, which in turn leads to a variation of the adjoint source $\delta_s f$ and a modification of the sensitivity to Earth structure. As an example, a variation in the source distribution δS_{nm} may affect the measurement of an amplitude difference. Consequently, the sensitivity of the measurement with respect to Earth structure will change.

Second, we observe changes in sensitivity to Earth structure because perturbations of the noise source distribution affect the nature of the forward field. While the adjoint field propagates the measured waveform differences back into the medium, the interaction with the forward field localizes the regions where perturbations of the medium may have caused the observed misfit. Changes in the noise sources may therefore affect the regions into which structural sensitivity is localized.

The different nature of the two contributions has implications for the solution of inverse problems based on ambient noise correlations. Through the design of suitable measurements, it may be possible to limit the perturbation of the measurement in response to changes of the noise source distribution. In this context, it is frequently argued that traveltime measurements are nearly unaffected by variations in noise source properties (e.g. Froment *et al.* 2010). However, the second contribution, that is the perturbation of the forward correlation fields, cannot be influenced through measurement design. While a suitably defined measurement may be nearly correct, its sensitivity to Earth structure may still be wrong.

4.3 The geometry of source-structure trade-offs

In order to gain more physical insight into eq. (39), we make a series of simplifying assumptions. First, we assume that the measurement itself is only weakly affected by the source perturbation, meaning that the terms involving the perturbation of the adjoint source, $\delta_s f$, can be neglected. This assumption can be justified for traveltime measurements such as those used in previous paragraphs for the computation of sensitivity kernels for noise sources and structure. Furthermore, we assume that the wavefield is acoustic, so that vector and tensor quantities are transformed to scalars. Finally, we limit ourselves to noise source perturbations that are point-localized at $\mathbf{x} = \mathbf{x}_0$, meaning that $\delta S(\mathbf{x}) = \delta S \delta(\mathbf{x} - \mathbf{x}_0)$. Under these assumptions, eq. (39) condenses to

$$\begin{aligned} \delta_s \delta_m \chi &= -2 \delta S \operatorname{Re} \int_{\omega=0}^{\infty} \int_{\mathbf{x} \in \oplus} \underbrace{G^\dagger(\mathbf{x}, \mathbf{x}_2) f^* [\delta_m \mathcal{L}_x G(\mathbf{x}, \mathbf{x}_0) G^*(\mathbf{x}_1, \mathbf{x}_0)]}_{\text{I}} d\mathbf{x} d\omega \\ &\quad - 2 \delta S \operatorname{Re} \int_{\omega=0}^{\infty} \int_{\mathbf{x} \in \oplus} \underbrace{G^\dagger(\mathbf{x}, \mathbf{x}_1) f [\delta_m \mathcal{L}_x G(\mathbf{x}, \mathbf{x}_0) G^*(\mathbf{x}_2, \mathbf{x}_0)]}_{\text{II}} d\mathbf{x} d\omega. \end{aligned} \quad (41)$$

The integral labelled I represents the interaction of the adjoint field $G^\dagger(\mathbf{x}, \mathbf{x}_2) f^*$ emitted from $\mathbf{x} = \mathbf{x}_2$ with the forward field $G(\mathbf{x}, \mathbf{x}_0) G^*(\mathbf{x}_1, \mathbf{x}_0)$ emitted from $\mathbf{x} = \mathbf{x}_0$ with a time delay of $|\mathbf{x}_1 - \mathbf{x}_0|/v$. Similarly, the second integral, labelled II, is the interaction between the adjoint field $G^\dagger(\mathbf{x}, \mathbf{x}_1) f$ emitted from $\mathbf{x} = \mathbf{x}_1$ with the forward field $G(\mathbf{x}, \mathbf{x}_0) G^*(\mathbf{x}_2, \mathbf{x}_0)$ emitted from $\mathbf{x} = \mathbf{x}_0$ with a time delay of $|\mathbf{x}_2 - \mathbf{x}_0|/v$. The potential scatterer positions \mathbf{x} where the integrals in eq. (41) are significantly different from zero are mostly determined by the stationary-phase regions.

Adopting the measurement from an earlier paragraph, the phase of the adjoint source f is approximately given by $i\omega|\mathbf{x}_1 - \mathbf{x}_2|/v$. The total phase of the integrand I is therefore approximated by

$$\frac{i\omega}{v} (-|\mathbf{x} - \mathbf{x}_2| - |\mathbf{x}_1 - \mathbf{x}_2| - |\mathbf{x} - \mathbf{x}_0| + |\mathbf{x}_1 - \mathbf{x}_0|). \quad (42)$$

For the phase of integrand I to be approximately stationary, we thus require

$$\underbrace{|\mathbf{x}_0 - \mathbf{x}| + |\mathbf{x} - \mathbf{x}_2|}_{\text{source} \rightarrow \text{scatterer} \rightarrow \text{receiver } 2} + \underbrace{|\mathbf{x}_2 - \mathbf{x}_1|}_{\text{correlation}} \approx \underbrace{|\mathbf{x}_0 - \mathbf{x}_1|}_{\text{source} \rightarrow \text{receiver } 1}. \quad (43)$$

Solutions \mathbf{x} to the approximate equality (43) only exist when the position \mathbf{x}_0 of the source perturbation is inside the narrow grey-shaded region of Fig. 4(a), characterized by $y \approx 0$ and $x \gtrsim x_2$. Intuitively, relation (43) means that a wave excited by the source perturbation at \mathbf{x}_0 and propagating to \mathbf{x}_1 should travel for about as long as a wave propagating from \mathbf{x}_0 to a scatterer at \mathbf{x} , from there to receiver \mathbf{x}_2 and finally also to receiver \mathbf{x}_1 . Provided that this condition is met, the stationary-phase region takes the shape of an ellipse around the line connecting \mathbf{x}_2 to the position of the source perturbation \mathbf{x}_0 .

Similarly for integrand, in eq. (41), the stationary-phase region is given by solutions \mathbf{x} to the approximate relation

$$\underbrace{|\mathbf{x}_0 - \mathbf{x}| + |\mathbf{x} - \mathbf{x}_1|}_{\text{source} \rightarrow \text{scatterer} \rightarrow \text{receiver } 1} \approx \underbrace{|\mathbf{x}_0 - \mathbf{x}_2|}_{\text{source} \rightarrow \text{receiver } 2} + \underbrace{|\mathbf{x}_2 - \mathbf{x}_1|}_{\text{correlation}}. \quad (44)$$

Relation (44) requires that the traveltime of a wave emitted by the source perturbation and propagating via the scatterer to receiver \mathbf{x}_1 approximates the traveltime of a wave travelling from the source perturbation to \mathbf{x}_2 and finally to \mathbf{x}_1 . The correlation of these two waves

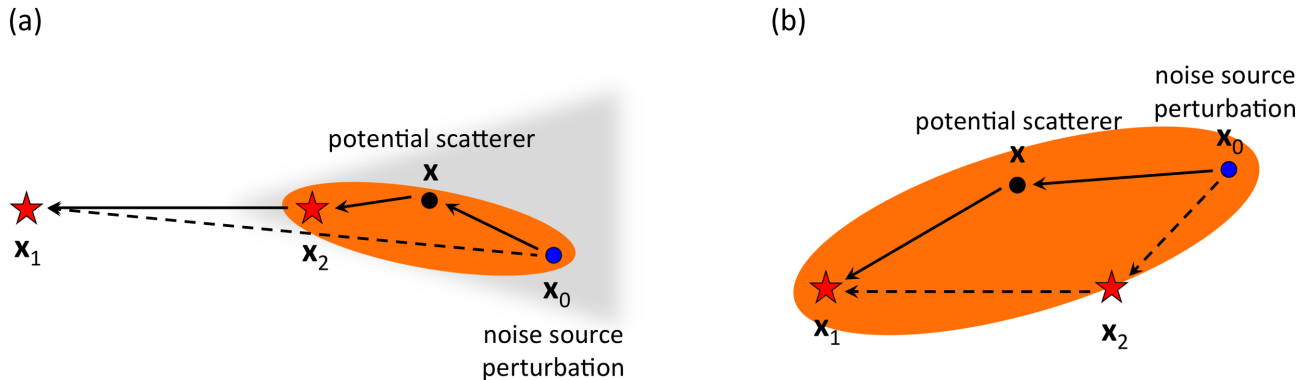


Figure 4. Illustration of the integrands I (panel a) and II (panel b) in eq. (41). The stationary-phase regions of the two integrands are marked in orange. Within the stationary-phase regions, a noise source perturbation at \mathbf{x}_0 can trade-off with a structural perturbation at \mathbf{x} . No stationary-phase region exists for integrand I when the noise source perturbation is outside the grey-shaded area behind receiver \mathbf{x}_2 .

would lead to a detectable waveform change inside the measurement window. As illustrated in Fig. 4(b), solutions to eq. (44) exist for source perturbations at any position \mathbf{x}_0 , and they take the form of an ellipse through \mathbf{x}_2 and around the line connecting the source perturbation at \mathbf{x}_0 to receiver \mathbf{x}_1 .

In summary, noise source perturbations at \mathbf{x}_0 may trade off with Earth structure located within two elliptical regions, one between the source perturbation at \mathbf{x}_0 and receiver \mathbf{x}_2 , and the other between the source perturbation and receiver \mathbf{x}_1 . For a given noise source perturbation, the positioning of the ellipses is primarily controlled by the measurement window, which translates into the dominant phase of the adjoint source; in our case $i\omega|\mathbf{x}_1 - \mathbf{x}_2|/v$. Shifting the measurement window would change the width of the ellipses. The type of measurement performed within the time window only controls the sensitivity pattern within the trade-off ellipses, but it does not affect their positioning.

4.4 Numerical examples for 2-D acoustic, attenuating media

Following the geometrical considerations of the previous section, we provide concrete examples for the trade-off kernel $\delta_c K$ introduced in eq. (40). In the interest of simplicity, we again limit ourselves to a 2-D acoustic, attenuating medium.

4.4.1 Position of the noise source perturbation

We commence our exploration of trade-off kernels by varying the position \mathbf{x}_0 of the point-localized noise source perturbation. In the following examples, the noise source perturbation has unit amplitude in the frequency band 0.005–0.035 Hz, and we set $Q = 200$.

The top panel of Fig. 5 shows the trade-off kernel $\delta_c K$ for a noise source perturbation located on the x -axis behind receiver \mathbf{x}_2 . As predicted by the stationary-phase argument in Section 4.3, trade-offs between the source-perturbation and structural heterogeneities occur within two elliptically-shaped regions, one connecting receiver \mathbf{x}_1 to the source perturbation at \mathbf{x}_0 , and the other connecting receiver \mathbf{x}_2 to \mathbf{x}_0 . In addition to source-structure trade-offs, the kernel indicates how sensitivity to velocity structure changes in response to a noise source perturbation at \mathbf{x}_0 .

As the noise source perturbation moves off the receiver-receiver line, that is out of the grey-shaded region in Fig. 4(a), the amplitude of the trade-off kernels is reduced. In accord with our previous stationary-phase considerations, the ellipse with foci \mathbf{x}_2 and \mathbf{x}_0 (integrand I) disappears, and the ellipse with foci \mathbf{x}_1 and \mathbf{x}_0 (integrand II) widens, while always passing through \mathbf{x}_2 . This is illustrated in the second and third rows of Fig. 5.

From varying the position of the noise source perturbation, we can draw two general conclusions: (i) Source-structure trade-offs in ambient noise correlations are a global phenomenon, meaning that there is no noise source perturbation that does not trade off with some Earth structure, and vice versa. This follows already from the fact that the stationary-phase relation (44) always has a solution. (ii) In our setup, source-structure trade-offs are strongest for noise source perturbations located directly behind receiver \mathbf{x}_2 , that is approximately in the non-zero regions of the noise source kernels (Fig. 2).

4.4.2 Frequency dependence of source-structure trade-offs

To analyse the frequency dependence of the source-structure trade-offs, we use the same setup as above but initially choose $Q = \infty$, meaning that attenuation is ignored. First, we note that the location of the stationary-phase regions in the trade-off kernel integral is independent of frequency. It follows that changes in the central frequency of the noise source perturbation mostly affect the amplitude of the trade-off kernels, and how rapidly they oscillate. This is illustrated in the top row of Fig. 6.

The stationary-phase arguments become increasingly irrelevant as the bandwidth of the noise source perturbation decreases. As shown in the middle row of Fig. 6, the trade-off kernel becomes increasingly oscillatory with decreasing bandwidth, eventually filling the whole

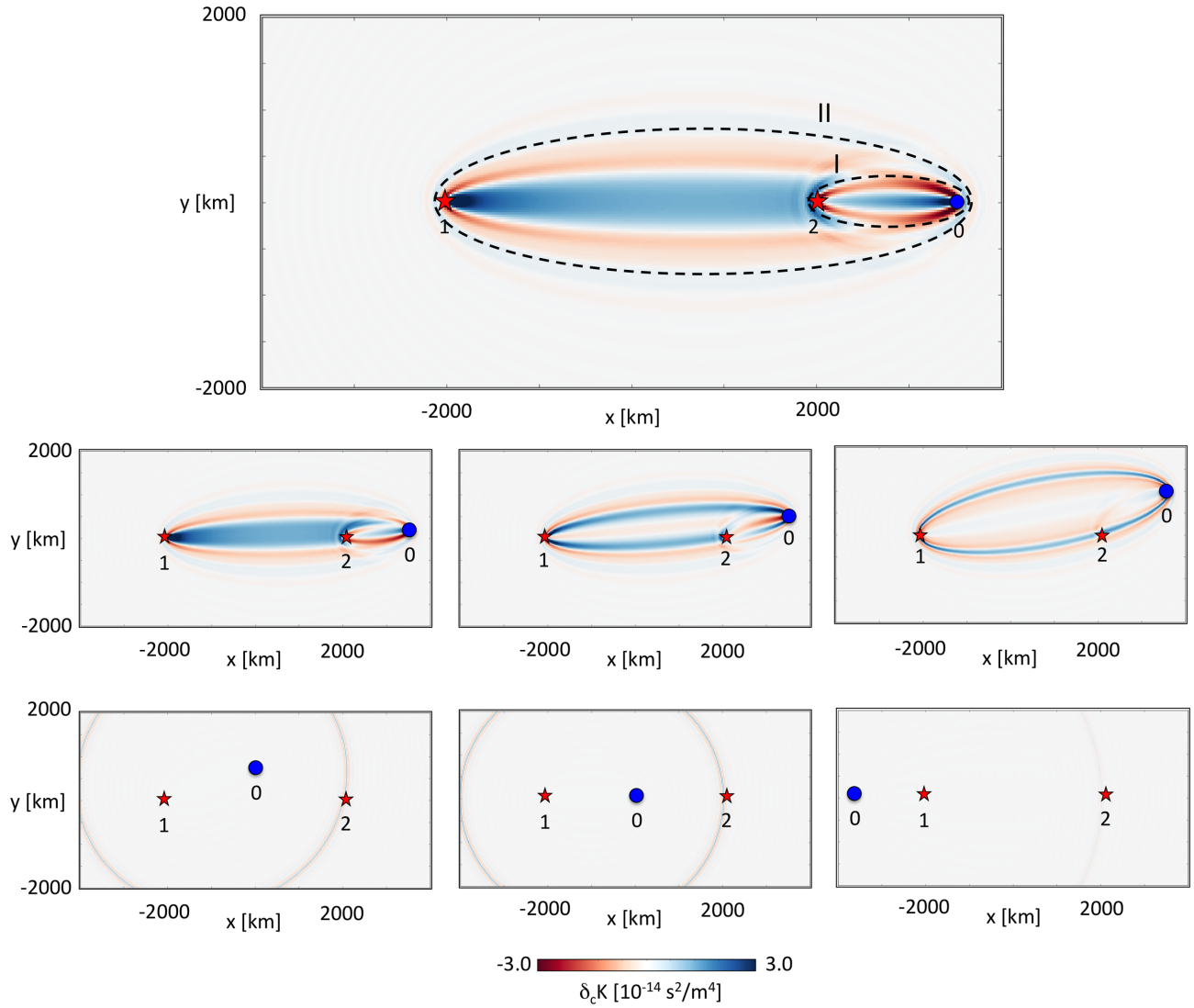


Figure 5. Trade-off kernels $\delta_c K$ for different positions x_0 of the noise source perturbation, indicated by the blue dot. Red stars mark receiver positions. The noise source perturbation as unit amplitude in the frequency band $0.005\text{--}0.035$ Hz, and $Q = 200$. Dotted ellipses in the top panel refer to the stationary-phase regions of integrands I and II in eq. (41).

domain with short-wavelength oscillations when the source perturbation is nearly monochromatic. This observation implies that far from the elliptical stationary-phase regions (Fig. 4) only small-scale structural heterogeneities can trade off with noise source perturbations. As illustrated in the bottom row, this statement is true independent of the position x_0 where the noise source is assumed to change.

4.4.3 Attenuation dependence of source-structure trade-offs

The attenuation dependence of source-structure trade-offs results from the presence of Q in the Green functions (eq. 12) that contribute to the trade-off kernel $\delta_c K$ from eq. (41). Furthermore, the adjoint source derived in Appendix A contributes a factor $\exp(\frac{\omega|x_1-x_2|}{2vQ})$. Accounting for the three Green functions that appear in eq. (41), it follows that

$$e^{\frac{\omega}{2vQ}(|x_1-x_2|-|x-x_{2/1}|-|x-x_0|-|x_{1/2}-x_0|)}. \quad (45)$$

We therefore expect, in accord with common intuition, that source-structure trade-offs are reduced as frequency increases and Q decreases. This behaviour can be seen in the numerical examples shown in the top and middle rows of Fig. 7. The effect of attenuation is particularly visible in the narrow-band kernels (middle row) because in the broad-band kernels (top row) the low-frequency components are only weakly affected, thus preventing the trade-off kernel amplitude from dropping quickly to zero.

A special situation arises when the configuration allows x to take values where

$$|x_1 - x_2| - |x_{1/2} - x_0| \approx |x - x_{2/1}| + |x - x_0|, \quad (46)$$

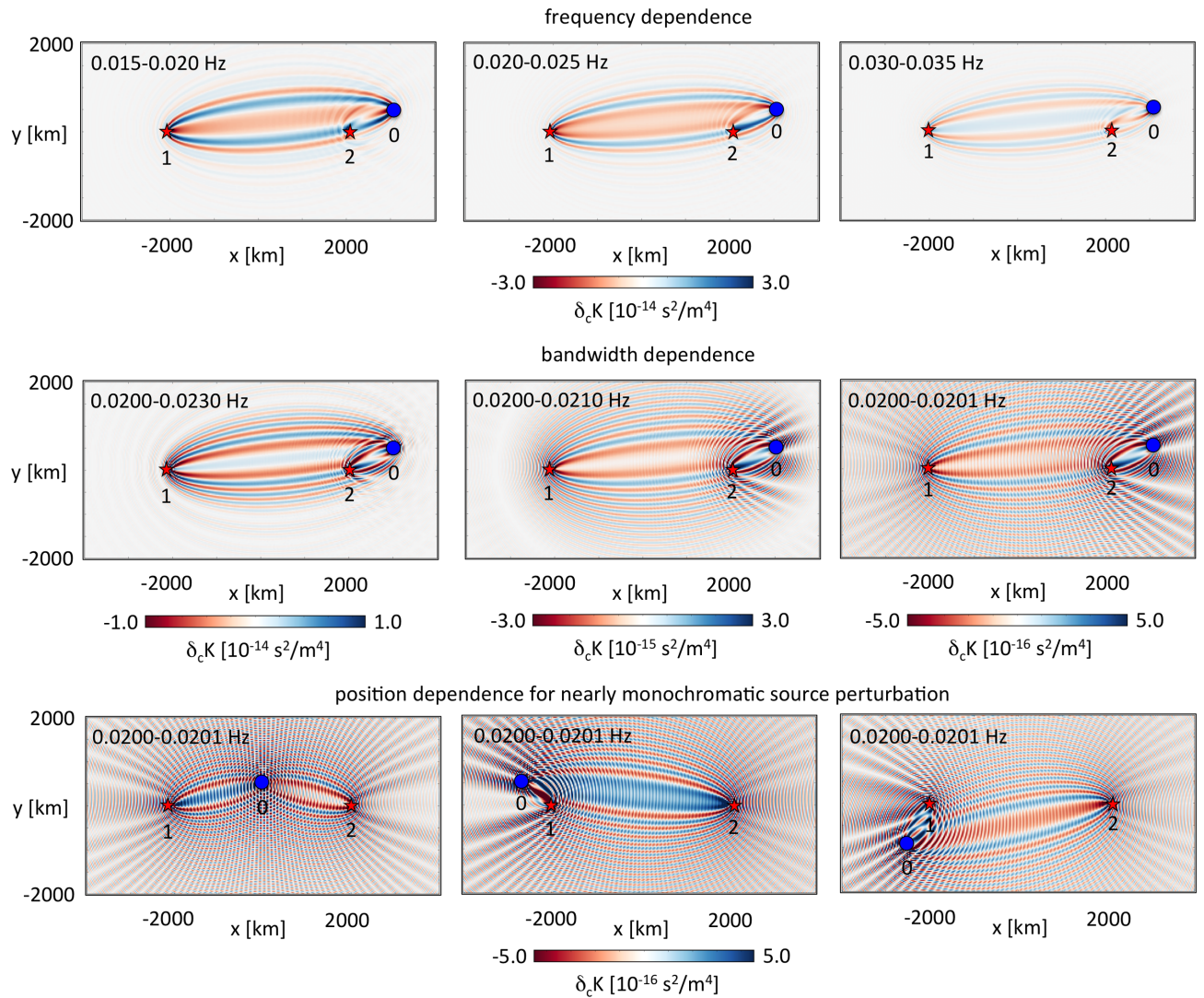


Figure 6. Frequency dependence of source-structure trade-offs. The blue dot marks the position of a potential noise source perturbation. Red stars indicate receiver positions. Top: trade-off kernel $\delta_c K$ for noise source perturbations with constant bandwidth of 5.0 mHz but with a frequency band shifting from 0.015–0.020 to 0.030–0.035 Hz. Middle: trade-off kernels $\delta_c K$ for a source bandwidth decreasing from 3.0 to 0.1 mHz. Bottom: trade-off kernel $\delta_c K$ for a small source bandwidth of 0.1 mHz and various positions of the source perturbation.

so that the exponent in eq. (45) is nearly zero for all frequencies. For relation (46) to hold, we require

$$|\mathbf{x}_1 - \mathbf{x}_2| \gtrsim |\mathbf{x}_1 - \mathbf{x}_0| + |\mathbf{x}_2 - \mathbf{x}_0|, \quad (47)$$

meaning that the noise source perturbation must be located near the line connecting both receivers. In such cases, source-structure trade-offs are unaffected by attenuation within narrow ellipsoidal regions that have \mathbf{x}_0 and $\mathbf{x}_{1/2}$ as foci. This phenomenon is illustrated in the bottom row of Fig. 7.

5 DISCUSSION

In the previous sections, we analysed trade-offs between Earth structure and noise sources in interstation ambient noise correlations. Our approach is based on the computation of off-diagonal Hessian elements \mathbf{H}_{sm} that describe the extent to which perturbations of noise sources can compensate for perturbations in Earth structure without changing the misfit beyond the measurement uncertainty.

While our derivation of \mathbf{H}_{sm} is general and valid for viscoelastic wavefields in any dimension, we make a series of simplifications in the examples in order to facilitate the analysis and the development of physical intuition. These simplifications include the following: (i) The medium is 2-D, acoustic, homogeneous and unbounded. The waves propagating in such a medium are a useful analogue only for surface waves but not for body waves. Furthermore, effects arising from elasticity and source directivity are ignored, meaning that the range of possible trade-offs is likely to be smaller than it would be in a 3-D viscoelastic Earth. (ii) We restrict ourselves to the measurement of traveltimes within the time window where the causal wave packet of the Green function appears. This limitation is a choice that we made in order to

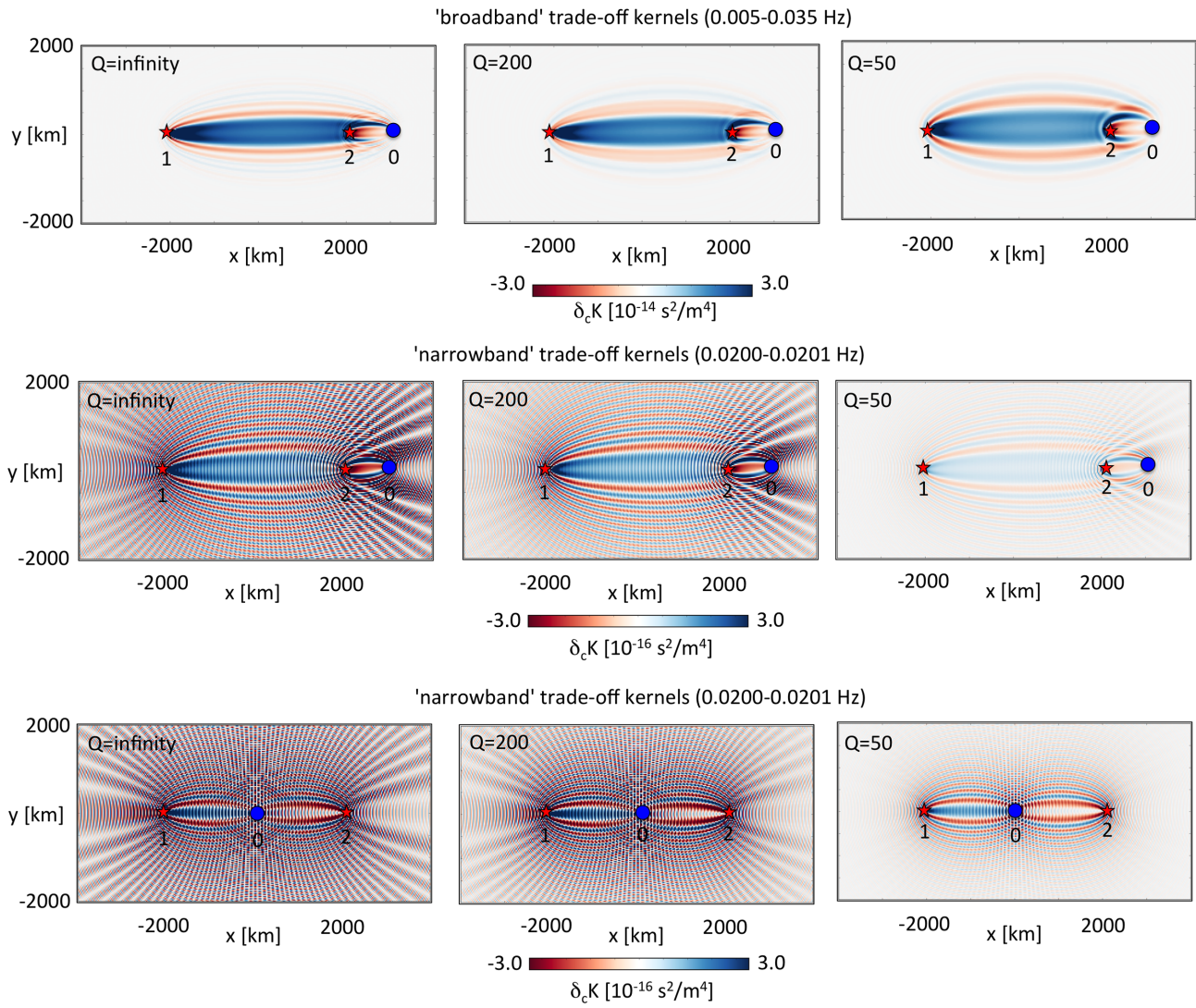


Figure 7. Attenuation dependence of source-structure trade-offs. The blue dot marks the position of a potential noise source perturbation. Red stars indicate receiver positions. Top: Trade-off kernels for different values of Q and a noise source perturbation that has unit amplitude within the frequency band 0.005–0.035 Hz. Middle: The same as above but for a noise source perturbation confined to the narrow frequency band 0.0200–0.0201 Hz. Bottom: The same as in the middle row but for a noise source perturbation located on the receiver–receiver line. As predicted, the source-structure trade-offs are nearly unaffected by attenuation within two narrow elliptical regions connecting x_0 to x_1 and x_2 , respectively.

keep the number of examples reasonable. It is further motivated by the fact that traveltimes of surface waves are by far the most common measurements on noise correlations, despite recent attempts to infer attenuation structure from amplitudes (e.g. Lawrence & Prieto 2011). (iii) In most of the examples, we ignore additional trade-offs that result from perturbations in the measurements induced by perturbations in the noise source. This simplification can be justified for traveltime measurements on the main arrival that are known to be only weakly affected by the noise source properties (e.g. Froment *et al.* 2010). In this sense, our analysis is conservative.

An aspect about which we did not make assumptions is the nature of the noise sources. These may be ocean and atmosphere interactions with the solid Earth, anthropogenic sources, or small-scale scatterers that excite a secondary wavefield. In this regard, our developments are general.

Current applications of ambient noise tomography are characterized by extensive data processing, examples of which may be found in Bensen *et al.* (2007), Groos *et al.* (2012) and Schimmel *et al.* (2011). Processing affects not only noise correlations themselves but also their sensitivity to Earth structure (Fichtner 2014). Being beyond the scope of this work, this effect is not studied in more detail. It may, however, be incorporated in the definition of the misfit functional χ , meaning that the analysis of processing effects is possible within the framework presented in the previous paragraphs.

In practical applications, source-structure trade-offs can never be avoided completely because there is no measurement that is exclusively sensitive to either noise sources or Earth structure. However, trade-offs can likely be reduced by clever measurement design, prior information on noise sources from non-seismological observations (Ardhuin *et al.* 2011), and by a joint inversion for sources and structure. Taking

advantage of the second-order adjoint approach presented in the previous paragraphs, the remaining trade-offs can at least be quantified, as it is done in imaging with deterministic sources (e.g. Fichtner & Trampert 2011; Fichtner & van Leeuwen 2015).

Finally, we note that quantitative trade-offs not only depend on the geometrical properties of the trade-off kernels but also on the configuration of the receiver array, the measurement errors, and on the prior knowledge of Earth structure and ambient noise sources. These experiment-specific factors are not considered in this study that attempts to derive general properties of source-structure trade-offs.

6 CONCLUSIONS

Within the limitations discussed in the previous paragraphs, we can draw the following main conclusions:

(1) While source-structure trade-offs may be reduced to some extent by clever measurement design, there are inherent trade-offs that can generally not be avoided. These inherent trade-offs, captured by the trade-off kernel $\delta_c K$ from eqs (40) and (41), may lead to a mispositioning of structural heterogeneities when the noise source distribution is unknown.

(2) When attenuation is weak, source-structure trade-offs in ambient noise correlations are a global phenomenon, meaning that there is no noise source perturbation that does not trade-off with some Earth structure, and vice versa. This is implied by the fact that the approximate relation (44) for the stationary-phase region of a trade-off kernel always has a solution. It follows that ambient noise tomography in a weakly attenuating Earth is strictly speaking a global-scale problem even when the receiver array occupies only a small region.

(3) The most significant source-structure trade-offs occur within the two elliptically shaped regions in Fig. 4 that connect a potential noise source perturbation to each one of the two receivers.

(4) Far from these elliptical regions, only small-scale structure can trade off against changes in the noise source. This follows from the fact that the trade-off kernels are highly oscillatory outside the stationary-phase regions.

(5) While source-structure trade-offs mostly decay with increasing attenuation, they are nearly unaffected by attenuation when the noise source perturbation is located near the receiver-receiver line.

ACKNOWLEDGEMENTS

The author gratefully acknowledges the hospitality of the Caltech SeismoLab where most of this manuscript was written. Many discussions with Shravan Hanasoge and Victor Tsai helped in the development of the mathematical symbolism and in the interpretation of the results. Furthermore, I would like to thank Laura Ermert and Korbinian Sager for inspiration, and the reviewers Pierre Boué and Paul Cupillard for their constructive criticism. This research was supported by the Swiss National Supercomputing Center (CSCS) in the form of the GeoScale and CH1 projects, by the Swiss National Science Foundation (SNF) under grant 200021_149143 and by the Netherlands Organisation for Scientific Research (VIDI grant 864.11.008).

REFERENCES

- Aki, K. & Richards, P., 2002. *Quantitative Seismology*, University Science Books.
- Ardhuin, F., Stutzmann, E., Schimmel, M. & Mangeney, A., 2011. Ocean wave sources of seismic noise, *J. geophys. Res.*, **116**, doi:10.1029/2011JC006952.
- Basini, P., Nissen-Meyer, T., Boschi, L., Casarotti, E., Verbeke, J., Schenck, O. & Giardini, D., 2013. The influence of nonuniform ambient noise on crustal tomography in Europe, *Geochem. Geophys. Geosyst.*, **14**, 1471–1492.
- Bath, M., 1968. *Mathematical Aspects of Seismology*, Elsevier.
- Bensen, G.D., Ritzwoller, M.H., Barmin, M.P., Levshin, A.L., Lin, F., Moschetti, M.P., Shapiro, N.M. & Yang, Y., 2007. Processing seismic ambient noise data to obtain reliable broad-band surface wave dispersion measurements, *Geophys. J. Int.*, **169**, 1239–1260.
- Brenguier, F., Campillo, M., Hazioannou, C., Shapiro, N.M., Nadeau, R.M. & Larose, E., 2008. Postseismic relaxation along the San Andreas fault at Parkfield from continuous seismological observations, *Science*, **321**, 1478–1481.
- Chen, P., 2011. Full-wave seismic data assimilation: Theoretical background and recent advances, *Pure appl. Geophys.*, **168**, 1527–1552.
- Cupillard, P. & Capdeville, Y., 2010. On the amplitude of surface waves obtained by noise correlation and the capability to recover the attenuation: a numerical approach, *Geophys. J. Int.*, **181**, 1687–1700.
- de Ridder, S.A.L., Biondi, B.L. & Clapp, R.G., 2014. Time-lapse seismic noise correlation tomography at Valhall, *Geophys. Res. Lett.*, **41**, 6116–6122.
- de Vos, D., Paulssen, H. & Fichtner, A., 2013. Finite-frequency sensitivity kernels from two-station surface wave measurements, *Geophys. J. Int.*, **194**, 1042–1049.
- Duputel, Z., Ferrazzini, V., Brenguier, F., Shapiro, N., Campillo, M. & Nercissian, A., 2009. Real time monitoring of relative velocity changes using ambient seismic noise at the Piton de la Fournaise volcano (La Réunion) from January 2006 to June 2007, *J. Volcanol. Geotherm. Res.*, **184**, 164–173.
- Fichtner, A., 2010. *Full Seismic Waveform Modelling and Inversion*, Springer.
- Fichtner, A., 2014. Source and processing effects on noise correlations, *Geophys. J. Int.*, **197**, 1527–1531.
- Fichtner, A., Bunge, H.-P. & Igel, H., 2006. The adjoint method in seismology - I. Theory, *Phys. Earth planet. Inter.*, **157**, 86–104.
- Fichtner, A. & Trampert, J., 2011. Resolution analysis in full waveform inversion, *Geophys. J. Int.*, **187**, 1604–1624.
- Fichtner, A. & van Leeuwen, T., 2015. Resolution analysis by random probing, *J. geophys. Res.*, in press.
- Froment, B., Campillo, M., Roux, P., Gouédard, P., Verdel, A. & Weaver, R.L., 2010. Estimation of the effect of nonisotropically distributed energy on the apparent arrival time in correlations, *Geophysics*, **75**, SA85–SA93.
- Groos, J.C., Bussat, S. & Ritter, J.R.R., 2012. Performance of different processing schemes in seismic noise cross-correlations, *Geophys. J. Int.*, **188**, 498–512.
- Gualtieri, L., Stutzmann, E., Capdeville, Y., Ardhuin, F.M., Schimmel, A.M. & Morelli, A., 2013. Modeling secondary microseismic noise by normal mode summation, *Geophys. J. Int.*, **193**, 1732–1745.

- Halliday, D. & Curtis, A., 2008. Seismic interferometry, surface waves and source distribution, *Geophys. J. Int.*, **175**, 1067–1087.
- Hanasoge, S.M., 2013a. Measurements and kernels for source-structure inversions in noise tomography, *Geophys. J. Int.*, **192**, 971–985.
- Hanasoge, S.M., 2013b. The influence of noise sources on cross-correlation amplitudes, *Geophys. J. Int.*, **192**, 295–309.
- Kennett, B.L.N., 2001. *The Seismic Wavefield: I. Introduction and Theoretical Development*, Cambridge Univ. Press.
- Kimman, W. & Trampert, J., 2010. Approximations in seismic interferometry and their effects on surface waves, *Geophys. J. Int.*, **182**, 461–476.
- Lawrence, J.W. & Prieto, G.A., 2011. Attenuation tomography in the western United States from ambient seismic noise, *J. geophys. Res.*, **116**, doi:10.1029/2010JB007836.
- Lobkis, O.I. & Weaver, R.L., 2001. On the emergence of the Green's function in the correlations of a diffuse field, *J. acoust. Soc. Am.*, **110**, 3011–3017.
- Luo, Y. & Schuster, G.T., 1991. Wave-equation traveltime inversion, *Geophysics*, **56**, 645–653.
- Malcolm, A.E., Scales, J. & van Tiggelen, B.A., 2004. Extracting the Green function from diffuse, equipartitioned waves, *Phys. Rev. E*, **70**, 015601-1–015601-4.
- Nishida, K., 2011. Two-dimensional sensitivity kernels for cross-correlation functions of background surface waves, *Comptes Rendus - Geoscience*, **343**, 584–590.
- Nishida, K., 2014. Source spectra of seismic hum, *Geophys. J. Int.*, **199**(1), 416–429.
- Nishida, K. & Fukao, Y., 2007. Source distribution of Earth's background free oscillations, *J. geophys. Res.*, **112**.
- Planes, T., Larose, E., Margerin, L., Rosetto, V. & Sens-Schönfelder, C., 2015. Decorrelation and phase shift of coda waves induced by local changes: multiple scattering approach and numerical validation, *Waves in Random and Complex Media*, **24**(2), 99–125.
- Rudin, W., 1966. *Real and Complex Analysis*, McGraw-Hill.
- Sabra, K.G., Gerstoft, P., Roux, P. & Kuperman, W.A., 2005. Surface wave tomography from microseisms in Southern California, *Geophys. Res. Lett.*, **32**, doi:10.1029/2005GL023155.
- Saygin, E. & Kennett, B.L.N., 2012. Crustal structure of Australia from ambient seismic noise tomography, *J. geophys. Res.*, **117**, doi:10.1029/2011JB008403.
- Schimmel, M., Stutzmann, E. & Gallart, J., 2011. Using instantaneous phase coherence for signal extraction from ambient noise data at a local to a global scale, *Geophys. J. Int.*, **184**, 494–506.
- Shapiro, N.M., Campillo, M., Stehly, L. & Ritzwoller, M., 2005. High resolution surface wave tomography from ambient seismic noise, *Science*, **307**, 1615–1618.
- Snieder, R., 2004. Extracting the Green's function from the correlation of coda waves: a derivation based on stationary phase, *Phys. Rev. E*, **69**, doi:10.1103/PhysRevE.69.046610.
- Snieder, R., Fan, Y., Slob, E. & Wapenaar, K., 2010. Equipartitioning is not sufficient for Green's function extraction, *Earthq. Sci.*, **23**, 403–415.
- Tarantola, A., 1988. Theoretical background for the inversion of seismic waveforms, including elasticity and attenuation, *Pure appl. Geophys.*, **128**, 365–399.
- Tromp, J., Tape, C. & Liu, Q., 2005. Seismic tomography, adjoint methods, time reversal and banana-doughnut kernels, *Geophys. J. Int.*, **160**, 195–216.
- Tromp, J., Luo, Y., Hanasoge, S. & Peter, D., 2010. Noise cross-correlation sensitivity kernels, *Geophys. J. Int.*, **183**, 791–819.
- Tsai, V.C., 2009. On establishing the accuracy of noise tomography traveltime measurements in a realistic medium, *Geophys. J. Int.*, **178**, 1555–1564.
- Tsai, V.C., 2010. The relationship between noise correlation and the green's function in the presence of degeneracy and the absence of equipartition, *Geophys. J. Int.*, **182**, 1509–1514.
- Tsai, V.C., 2011. Understanding the amplitudes of noise correlation measurements, *J. geophys. Res.*, **116**, doi:10.1029/2011JB008483.
- Wapenaar, K., 2004. Retrieving the elastodynamic Green's function of an arbitrary inhomogeneous medium by cross correlation, *Phys. Rev. Lett.*, **93**, 254301.
- Wapenaar, K. & Fokkema, J., 2006. Green's function representations for seismic interferometry, *Geophysics*, **71**, S133–S146.
- Weaver, R.L. & Lobkis, O.I., 2004. Diffuse fields in open systems and the emergence of Green's function, *J. acoust. Soc. Am.*, **116**, 2731–2734.
- Woodard, M.F., 1997. Implications of localized, acoustic absorption for heliotomographic analysis of sunspots, *Astrophys. J.*, **485**, 890–894.

APPENDIX A: MEASUREMENT FUNCTIONALS AND THEIR VARIATION

To first demonstrate the statement from eq. (14), we note that the real-valued misfit functional χ is a function of the interstation correlation $C_{ij}(\mathbf{x}_1, \mathbf{x}_2, \omega)$:

$$\chi = \chi[C_{ij}(\mathbf{x}_1, \mathbf{x}_2, \omega)]. \quad (\text{A1})$$

The first variation of χ in the direction of the infinitesimal perturbation $\delta C_{ij}(\mathbf{x}_1, \mathbf{x}_2, \omega)$ is, by definition of the first variation, a linear functional in $\delta C_{ij}(\mathbf{x}_1, \mathbf{x}_2, \omega)$ itself. As a consequence of Riesz' theorem (e.g. Rudin 1966), this functional can be uniquely represented by the scalar product with some function $f(\omega)$, that is by the integral

$$\delta\chi = \int_{-\infty}^{\infty} \delta C_{ij}(\mathbf{x}_1, \mathbf{x}_2, \omega) f(\omega) d\omega. \quad (\text{A2})$$

Since $\delta C_{ij}(\mathbf{x}_1, \mathbf{x}_2, \omega)$ is the Fourier transform of the real-valued time-domain perturbation $\delta C_{ij}(\mathbf{x}_1, \mathbf{x}_2, t)$, we also have

$$\delta\chi = \int_{-\infty}^{\infty} \delta C_{ij}^*(\mathbf{x}_1, \mathbf{x}_2, \omega) f^*(\omega) d\omega = \int_{-\infty}^{\infty} \delta C_{ij}(\mathbf{x}_1, \mathbf{x}_2, -\omega) f^*(\omega) d\omega = \int_{-\infty}^{\infty} \delta C_{ij}(\mathbf{x}_1, \mathbf{x}_2, \omega) f^*(-\omega) d\omega. \quad (\text{A3})$$

It follows from eq. (A3) that $f(-\omega) = f^*(\omega)$, meaning that $f(\omega)$ can be interpreted as the Fourier transform of a real-valued function as well. Taking advantage of this result, we can rewrite eq. (A2) as an integral over positive frequencies only:

$$\delta\chi = 2 \operatorname{Re} \int_0^{\infty} \delta C_{ij}(\mathbf{x}_1, \mathbf{x}_2, \omega) f(\omega) d\omega. \quad (\text{A4})$$

This is the result from eq. (14). From a physics perspective, the function $f(\omega)$ plays the role of a frequency-domain adjoint source. In the following paragraphs, we derive the specific expression for f when the measurements are cross-correlation time shifts (Luo & Schuster 1991).

In the time domain, the correlation time shift is defined as the time T where the correlation between synthetic and observed correlation functions attains its (global) maximum, that is

$$\chi = T = \arg \max \int \tilde{C}_{ij}(\tau) \tilde{C}_{ij}^{(0)}(t + \tau) d\tau. \quad (\text{A5})$$

For $T > 0$, the synthetic \tilde{C}_{ij} is advanced relative to the data $\tilde{C}_{ij}^{(0)}$, and vice versa. The definition of T implies that the time derivative of the correlation integral in eq. (A5) is zero for $t = T$:

$$\int \tilde{C}_{ij}(\tau) \dot{\tilde{C}}_{ij}^{(0)}(T + \tau) d\tau = 0. \quad (\text{A6})$$

Applying implicit function differentiation to eq. (A6) gives the first variation of T :

$$\delta T = \frac{\int \delta \tilde{C}_{ij}(\tau) \dot{\tilde{C}}_{ij}^{(0)}(T + \tau) d\tau}{\int \dot{\tilde{C}}_{ij}(\tau) \dot{\tilde{C}}_{ij}^{(0)}(T + \tau) d\tau}. \quad (\text{A7})$$

Writing the integrals in the frequency domain, results in the following expression for δT :

$$\delta T = -i \frac{\int \omega e^{-i\omega T} \delta C_{ij} C_{ij}^{(0)*} d\omega}{\int \omega^2 e^{-i\omega T} C_{ij} C_{ij}^{(0)*} d\omega}. \quad (\text{A8})$$

Eq. (A8) can again be brought into the generic form

$$\delta T = \operatorname{Re} \int \delta C_{ij}(\mathbf{x}_1, \mathbf{x}_2, \omega) f(\omega) d\omega, \quad (\text{A9})$$

with $f(\omega)$ given by

$$f(\omega) = -i \frac{\omega e^{-i\omega T} C_{ij}^{(0)*}}{\int \omega^2 e^{-i\omega T} C_{ij} C_{ij}^{(0)*} d\omega}. \quad (\text{A10})$$

Under the common assumption that the time-shifted data $\tilde{C}_{ij}^{(0)}(T + t)$ are approximately equal to the synthetics $\tilde{C}_{ij}(t)$, eq. (A10) can be simplified to

$$f(\omega) = -i \frac{\omega C_{ij}^*}{\int \omega^2 |C_{ij}|^2 d\omega}. \quad (\text{A11})$$

APPENDIX B: GREEN'S THEOREM

The Green function $\mathbf{G}_j(\mathbf{x}, \xi)$ with vector components $G_{ij}(\mathbf{x}, \xi)$ is the solution of the governing equations when the right-hand side equals a point-localized force at position ξ in j -direction, that is

$$\mathcal{L}_x \mathbf{G}_j(\mathbf{x}, \xi) = \mathbf{e}_j \delta(\mathbf{x} - \xi), \quad (\text{B1})$$

with \mathcal{L}_x being a linear forward modelling operator in the frequency domain acting on the spatial variable \mathbf{x} . The first variation of the i -component of \mathbf{G}_j is

$$\delta G_{ij}(\mathbf{x}, \xi) = \int_{\mathbf{x}' \in \oplus} \mathbf{e}_i \cdot \delta \mathbf{G}_j(\mathbf{x}', \xi) \delta(\mathbf{x} - \mathbf{x}') d\mathbf{x}'. \quad (\text{B2})$$

We can eliminate $\delta \mathbf{G}_j$ from eq. (B2) using the variation of eq. (B1), which is given by

$$\delta \mathcal{L}_{x'} \mathbf{G}_j(\mathbf{x}', \xi) + \mathcal{L}_{x'} \delta \mathbf{G}_j(\mathbf{x}', \xi) = \mathbf{0}. \quad (\text{B3})$$

Multiplying (B3) by the test field $\mathbf{u}^\dagger(\mathbf{x}')$, integrating over space and adding the result to eq. (B2), gives

$$\delta G_{ij}(\mathbf{x}, \xi) = \int_{\mathbf{x}' \in \oplus} \mathbf{e}_i \cdot \delta \mathbf{G}_j(\mathbf{x}', \xi) \delta(\mathbf{x} - \mathbf{x}') d\mathbf{x}' + \int_{\mathbf{x}' \in \oplus} \mathbf{u}^\dagger(\mathbf{x}') \cdot [\delta \mathcal{L}_{x'} \mathbf{G}_j(\mathbf{x}', \xi)] d\mathbf{x}' + \int_{\mathbf{x}' \in \oplus} \mathbf{u}^\dagger(\mathbf{x}') \cdot [\mathcal{L}_{x'} \delta \mathbf{G}_j(\mathbf{x}', \xi)] d\mathbf{x}'. \quad (\text{B4})$$

Invoking the adjoint $\mathcal{L}_{x'}^\dagger$ of the forward modelling operator $\mathcal{L}_{x'}$, we can rearrange eq. (B4) as follows:

$$\delta G_{ij}(\mathbf{x}, \xi) = \int_{\mathbf{x}' \in \oplus} \delta \mathbf{G}_j(\mathbf{x}', \xi) \cdot [\mathbf{e}_i \delta(\mathbf{x} - \mathbf{x}') + \mathcal{L}_{x'}^\dagger \mathbf{u}^\dagger(\mathbf{x}')] d\mathbf{x}' + \int_{\mathbf{x}' \in \oplus} \mathbf{u}^\dagger(\mathbf{x}') \cdot [\delta \mathcal{L}_{x'} \mathbf{G}_j(\mathbf{x}', \xi)] d\mathbf{x}'. \quad (\text{B5})$$

Forcing

$$\mathcal{L}_x^\dagger \mathbf{u}^\dagger(\mathbf{x}') = -\mathbf{e}_i \delta(\mathbf{x} - \mathbf{x}') \quad (\text{B6})$$

determines the test field $\mathbf{u}^\dagger(\mathbf{x}')$ to be the negative adjoint Green function with unit force in i -direction at position \mathbf{x} , that is

$$\mathbf{u}^\dagger(\mathbf{x}') = -\mathbf{G}_i^\dagger(\mathbf{x}', \mathbf{x}). \quad (\text{B7})$$

With the help of (B6) and (B7), the variation of the Green function, $\delta G_{ij}(\mathbf{x}, \xi)$, then condenses to

$$\delta G_{ij}(\mathbf{x}, \xi) = - \int_{\mathbf{x}' \in \oplus} \mathbf{G}_i^\dagger(\mathbf{x}', \mathbf{x}) \cdot [\delta \mathcal{L}_{\mathbf{x}'} \mathbf{G}_j(\mathbf{x}', \xi)] d\mathbf{x}'. \quad (\text{B8})$$

This is the desired expression for the first variation of the Green function that only requires the easily computable first variation of the forward modelling operator $\mathcal{L}_{\mathbf{x}}$.